

archives
of thermodynamics

Vol. **32**(2011), No. 3, 175–190

DOI: 10.2478/v10173-011-0021-5

Application of CFD technique for modelling of the thermoacoustic engine

SEBASTIAN RULIK*
LESZEK REMIORZ
SŁAWOMIR DYKAS

Silesian University of Technology, Institute of Power Engineering and Turbomachinery, ul. Konarskiego 18, 44-100 Gliwice, Poland

Abstract The paper is concerned with an important issue from the field of thermoacoustics – the numerical modelling of the flow field in the thermoacoustic engine. The presented way of modelling is based on the solution to fundamental fluid mechanics equations that govern the flow of compressible, viscous, and heat-transferring gas. The paper presents the way of modelling the thermoacoustic engine, the way of conducting calculations and the results which illustrate the correctness of the selected computational technique.

Keywords: Thermoacoustic engine; Thermoacoustic regiferator; Thermoacoustic; CFD

1 Introduction

Sound can be produced not only by vibrating bodies but also by a non-stationary flow field or a temperature gradient. Thermoacoustics deals with the study of the generation of acoustic waves whose source is the heat flow caused by a forced temperature gradient. The history of thermoacoustic devices goes back to the 19th century. The phenomenon of sound generation caused by a temperature gradient was first observed in glass-works. In the process of glass blowing, the heated glass tubes which were closed at

*Corresponding author. E-mail address: sebastian.rulik@polsl.pl

one end emitted a characteristic tonal sound. The theoretical basics of this field of acoustics were developed by Rayleigh [1]. His research led to the formulation of the fundamental principle of thermoacoustics. It states that in order to excite and maintain acoustic vibrations, heat should be delivered to the working agent at the moment of its largest compression, and collected at its expansion. The compression and expansion stages are related to the course of the acoustic wave which varies with time. The process can also be reversed and then the produced acoustic wave can generate a temperature gradient.

Further research to develop the theoretical basics and a mathematical description of the phenomenon mentioned above was done, among others, by Rott [2]. He developed the one-dimensional linear theory. In the 80s and 90s of the last century, Weatley and Swift [3,4] from “Los Alamos National Laboratory” in the USA made a considerable contribution to the development of theories in the field of thermoacoustics. The theoretical basis which they presented gives good results in the case of an analysis and design of devices operating at relatively small values of the acoustic pressure amplitude, for which the acoustic pressure – average working pressure ratio is smaller than 3%. In many cases, due to its high sensitivity to operating conditions, thermoacoustic equipment requires an analysis of operation under changing conditions, as well as an application of an optimisation process at its design. In a situation like this, the one-dimensional linear model shows many advantages. Today however, modern thermoacoustic equipment can work at higher values of the acoustic pressure amplitude. In this case, the linear theory based on the one-dimensional model fails. The model does not account for many additional factors which could have a significant impact on the quality of obtained results. These are related mainly to the determination of the influence of viscosity on the formation of the boundary layer, as well as of the impact of turbulences on the flow structure and generation of losses.

A further advancement in the field of thermoacoustic equipment was possible owing to the work of Feldman (1966) and Swift (1988), who used an additional component in the form of a porous body (stack) whose task was to exchange heat with the flowing gas. The component allowed a delivery of a specific portion of energy to the possibly greatest volume of the flowing gas, thus contributing to a substantial improvement in efficiency, and an increase in output power.

At present, the tools of the computational fluid dynamics (CFD) allow

a detailed analysis of the operation of thermoacoustic equipment. The solution to Navier-Stokes equations and the application of a turbulence model to model turbulent viscosity make it possible to determine the exact flow structure together with flow losses and any nonlinearities that might appear in the flow. This, however, involves a substantial increase in the time needed for the calculations and a need for more equipment resources. Examples of the application of the tools of the computational fluid dynamics, including commercial codes, for the analysis of thermoacoustic phenomena can be found, among others, in the works of Hantschk and Vortmeyer [5], Zoontjens [6] and Zink [7]. Therefore, the present application of the computational fluid dynamics in research related to thermoacoustics seems to be another stage to build a computational model which would be as precise and reliable as possible. The Authors have essential experience in the use of the tools of the CFD for the analysis of aeroacoustic problems related to modelling the generation and propagation of sound generated by a non-stationary flow field [8].

The principal aim of this paper is a numerical analysis of thermoacoustic phenomena which occur in the thermoacoustic engine. The application of the CFD methods to analyse the thermoacoustic effect was also a subject of the Authors' consideration earlier [9]. The applied numerical model is based on the solution to the fundamental equations that govern the gas flow, the solutions to the equations of conservation of mass, energy and momentum. The presented studies were all carried out with the use of the Ansys-CFX12 commercial CFD code.

2 Numerical modelling of the thermoacoustic engine

The thermoacoustic engine (Fig. 1) is usually constructed of a tube which is closed at one end; the other end may be closed with a piston, or a piezoelectric component can be placed there to generate electricity. In the case of laboratory tests, the usual study subject is a tube with the other end open to the surroundings.

For the thermoacoustic engine, the average velocity of the agent flow is always zero, and in the engine itself, the agent motion is caused only by an acoustic wave, making all the gas particles oscillate around the equilibrium position. This results from the fact that the thermoacoustic engine is open to the surroundings at one end only. The other end, which usually is closer

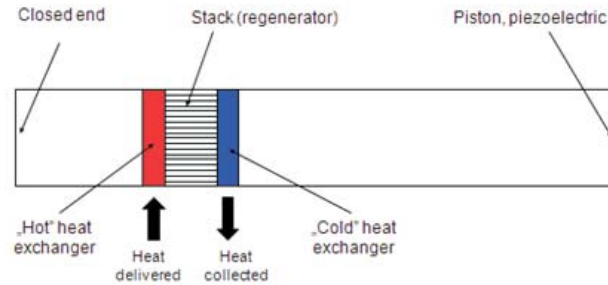


Figure 1. The thermoacoustic engine and its basic components.

to the heat exchanger itself, is always closed. As a result, only a quarter of the standing wave is produced in the thermoacoustic engine.

2.1 Assumptions

Figure 1 presents the basic diagram of the thermoacoustic engine, whereas Fig. 2 illustrates the computational area adopted for the numerical analysis. The basic components of the thermoacoustic engine are: regenerator (stack), two exchangers and a resonance tube. In the case of numerical model, the configuration was slightly simplified.

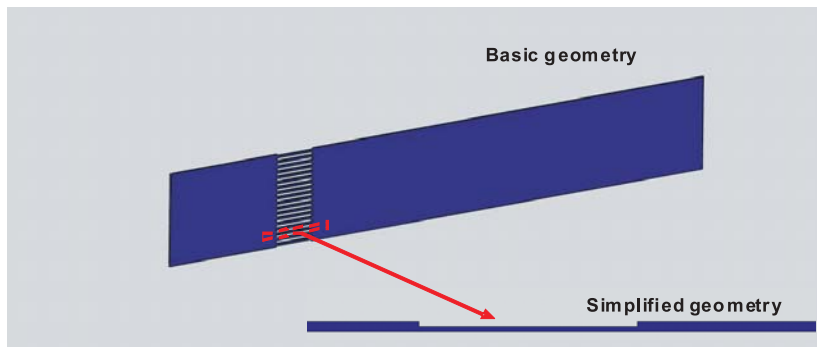


Figure 2. Diagram of the computational area geometry adopted for the analysis.

The presented model contains only one heat exchanger which replaces both the regenerator (stack) and the additional heat exchangers. A temperature distribution is set on the surface of the heating components along its

length. Additionally, various configurations of the adopted computational domain were examined within the framework of the analysis. The computational area included the analysis of the entire heat exchanger, as well as its individual components.

The impact of the adopted computational domain on the value of the basic parameters of the thermoacoustic engine operation was also studied. Figure 3 presents the basic dimensions and the location of one heating component of the heat exchanger. The whole device is 150 mm long, and is open to the surroundings only on the right side. The presented device can also work at pressures higher than atmospheric pressure. In this case however, the device has to be closed, and the mouth of the resonance tube has to be designed so that the velocity antinode will still be related to the section of the resonance tube mouth. The heat exchanger itself is at a 30 mm distance from the closed left side of the device.

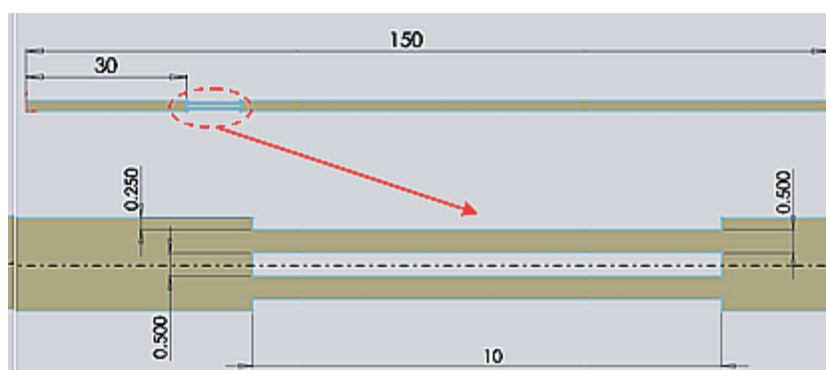


Figure 3. Basic dimensions of the thermoacoustic engine with a heat exchanger.

Figure 4 shows the boundary conditions adopted during the numerical analysis. Symmetry conditions were assumed on the upper and bottom edge of the computational domain for an analysis of only a sector of the heat exchanger.

The no-slip wall boundary condition was adopted only within the heat exchanger. Most of the conducted analyses which were related to the impact of both time and space discretisation, as well as to the impact of individual parameters on the operation of the thermoacoustic engine, were made with the use of the computational domain presented in Fig. 4. The computational area adopted in this way allowed a substantial shortening of the time of the

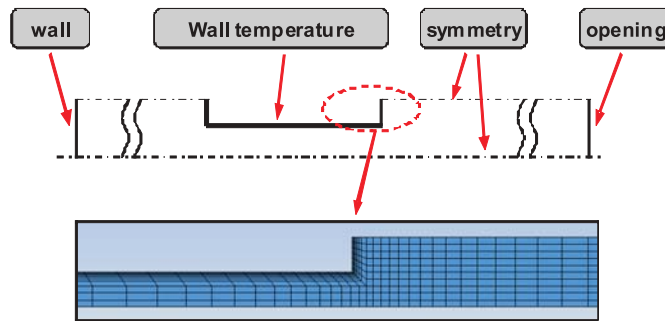


Figure 4. Adopted conditions for the calculations of the thermoacoustic engine.

calculations, and a more extensive number of analyses.

The adopted temperature distribution on the surface of the heat exchanger along its length was determined according to the following relation [7]:

$$T(x) = 1000 - \left[500 + 200 \cos \left(\frac{\pi x}{0.01} \right) \right]. \quad (1)$$

The temperature distribution adopted in this way causes that the maximum value of temperature for $x = 0.03$ m is 700 K, and it decreases along the length of the exchanger to the value of 300 K for $x = 0.04$ m.

The adopted temperature distribution of the surface of the heat exchanger along its length is presented in Fig. 5. The course is also a part of a sinusoid. Distance x in this case is measured according to Fig. 3.

2.2 Algorithm for the simulation of the thermoacoustic engine

Numerical modelling of the flow which varies with time requires, apart from the use of sophisticated numerical algorithms, an appropriate way of performing calculations that will ensure a fast and stable solution. The initial distribution of the flow field parameters used for non-stationary calculations is also essential for this type of calculations.

Table 1 presents the basic data adopted during the stationary and non-stationary analysis. The properties of air were based on Clapeyron equation. The specific heat capacity of air was constant. However, the values of thermal conductivity and dynamic viscosity were based on the Sutherland formula.

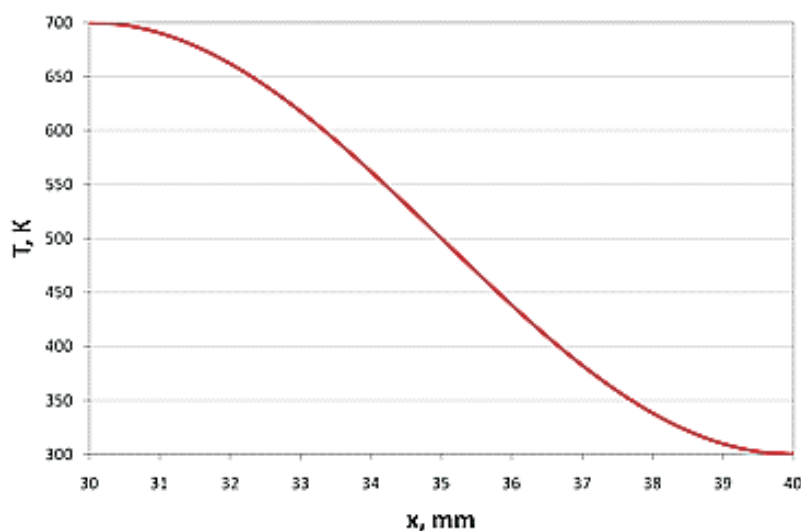


Figure 5. The adopted temperature distribution along the length of the heat exchanger.

Table 1. Data adopted for the numerical analysis of the thermoacoustic engine.

| | |
|--|------------------------------------|
| Gas | air, ideal gas |
| Time step | 10^{-5} s |
| Temperature at the outlet | 300 K |
| Heat exchanger wall temperature | according to dependence (1) |
| Reference pressure | 1 atm |
| Pressure at the inlet and outlet | 0 Pa |
| Turbulence model | KE |
| Space discretisation | high-resolution scheme |
| Time discretisation | second-order accuracy Euler scheme |
| Velocity and temperature at the outlet (stationary solution) | $v=0.01$ m/s, $T=300$ K |
| Velocity at the inlet (non-stationary solutions) | $v=0$ (wall) |

A small average velocity value of 0.01 m/s and the inlet temperature of 300 K were assumed for the stationary solution. For this reason, the value of velocity at the inlet to the thermoacoustic engine was assumed at the place of the previous boundary condition of zero wall velocity. Assuming the above-mentioned average velocity of the flow, the distribution of the

temperature field is presented in Fig. 6. It can be noticed that even a small value of the set velocity makes the device heat to the temperature of approx. 600 K only in the vicinity of the heat exchanger. At the outlet area the temperature value is 300 K. Assuming the zero value of the average velocity, the entire area on the left of the exchanger would heat to the temperature of 700 K, and the temperature on the right of the exchanger, i.e. in the area of the resonance tube, would be 300 K. However, the conducted studies showed that the initial distribution for the non-stationary analysis presented in Fig. 6 caused a better excitation of the sound wave and a faster stabilisation of the determined acoustic vibration amplitude.

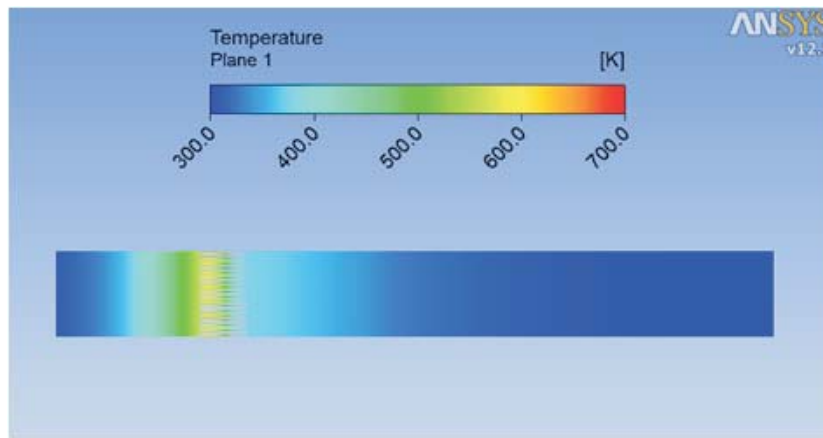


Figure 6. Initial distribution of the temperature field for the thermoacoustic engine.

The next stage in calculations is introduction of the pressure pulse into the stationary solution, assuming at the same time a very small time step for the energy equation. This causes that the distribution of pressure along the length of the thermoacoustic engine resembles the distribution of the acoustic wave pressure, while the temperature field remains unchanged.

The distribution of the pressure field is presented in Fig. 7. It can be noticed that the pressure decreases abruptly in the area of the heat exchanger itself from the assumed value of 10 Pa to the value of 0 Pa (compared to the reference pressure). At the same time, there is no fall in pressure along the tube length itself. This is related to the assumed conditions of symmetry for the upper and bottom edge of the sector of the thermoacoustic engine under consideration.

The simultaneous introduction of the pressure pulse entails also a change

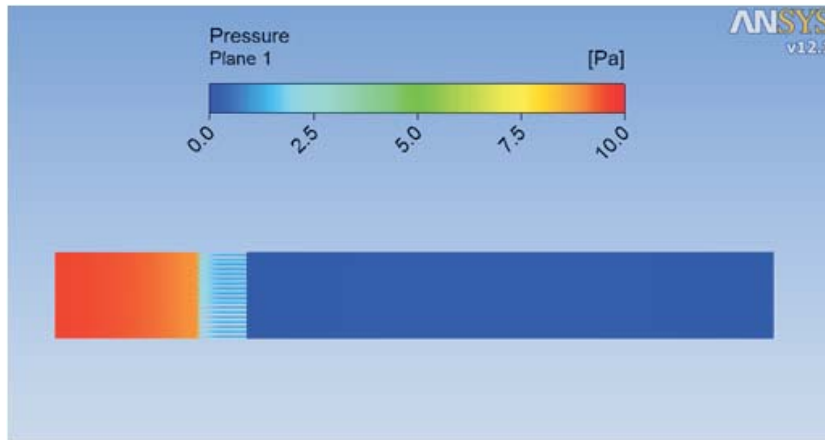


Figure 7. Initial distribution of pressure for the analysis of the thermoacoustic engine.

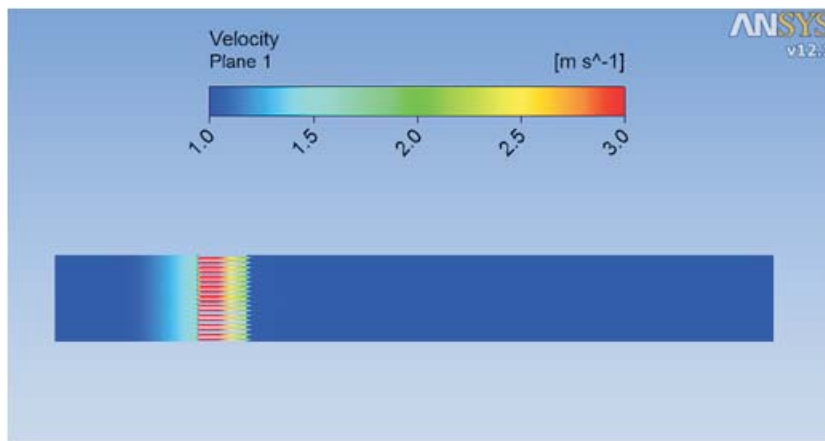


Figure 8. Initial distribution of velocity for the analysis of the thermoacoustic engine.

in the velocity field presented in Fig. 8. In this case, the maximum velocity value occurs in the area of the heat exchanger itself and is approx. 3 m/s.

A non-stationary analysis was conducted on the basis of the initial distribution prepared in this way. The process of the acoustic wave excitation is presented in Fig. 9. The basic time step of $1e-5$ was adopted for non-stationary calculations. The analysis included 60 thousand time steps (0.6 s). It can be noticed that in the initial stage of the acoustic wave excitation the sinusoid course of the acoustic wave is considerably

disturbed. However, the pressure course gradually smooths out, and after around 2 thousand iterations it approximates a sinusoid. Then, the acoustic vibration amplitude increases slowly in the following 20 thousand iterations and reaches a value of approx. 1800 Pa. From that moment on, a substantial rise in the vibration amplitude can be observed, which stabilises after approx. 40 thousand iterations at the level of 10 kPa.

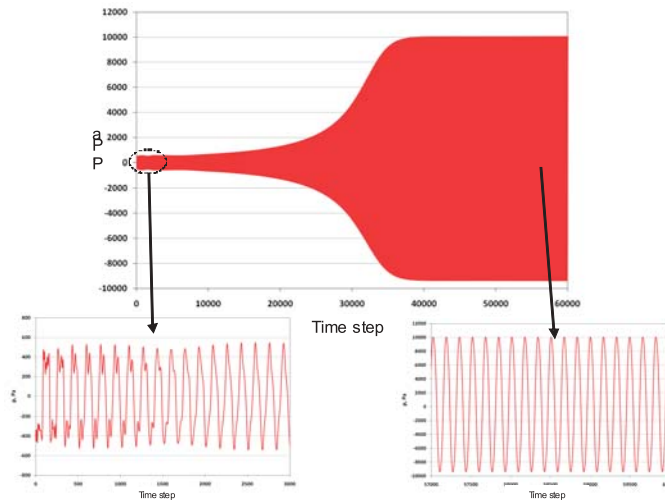


Figure 9. The process of the acoustic wave excitation for the thermoacoustic engine.

Figures 10 and 11 present distribution of the acoustic pressure and of the component v_x of velocity along the length of the thermoacoustic engine for individual phases of one full period T of vibration. The characteristics were determined along the line passing through a point located in the middle of the distance between the heat exchanger wall and the adopted plane of symmetry. In this case, the maximum velocity value is approx. 23 m/s. As it was stated before, the pressure amplitude is equal to 10 kPa.

A significant difference between the momentary characteristics of the pressure and velocity distributions appears in the heat exchanger area. In case of the pressure characteristic, the impact of the heat exchanger itself on the pressure distribution is small. For the velocity characteristics, however, there is a substantial increase in velocity which can be of the order of as much as 10 m/s. This is related to the use of a very narrow heat exchanger passages with a height of only 0.5 mm. It can also be noticed in Fig. 10 that small acoustic pressure oscillations around the average pressure value appear

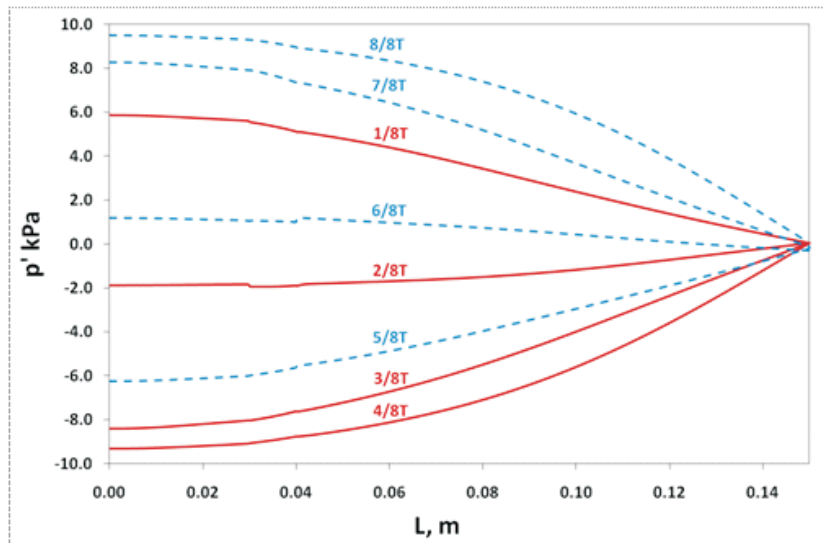


Figure 10. Distribution of instantaneous pressure depending on the length of the thermoacoustic engine ($T=1.6 \cdot 10^{-3}$ s).

in the outlet section of the thermoacoustic engine, despite the fact that a pressure node should be expected in this particular place. These oscillations, however are small. They are of the order of a few dozen pascals.

Additionally, the more detailed model of thermoacoustic engine was developed. This model consists of six heating elements of heat exchanger. Moreover, the no-slip wall boundary condition was applied for the top and bottom edge of the resonator. It allows to estimate the influence of viscous effects on the amplitude of acoustic wave. Table 2 presents the comparison of the velocity and pressure amplitude obtained in case of the simplified and detailed model of thermoacoustic engine. The pressure amplitude was determined in the closed end of the device where the pressure antinode appears. However, the velocity amplitude was specified at the open end where the velocity antinode is located. The relative error between both models is equal to 17%. The large difference between obtained results is associated with the viscous drag along the resonator. It has to be mentioned that the detailed model still does not reflect the real model which may consist of a few dozens of heating elements. However, the modelling of additional heating elements significantly increases the computational time. Due to this fact, it seems to be reasonable to use the simplified model

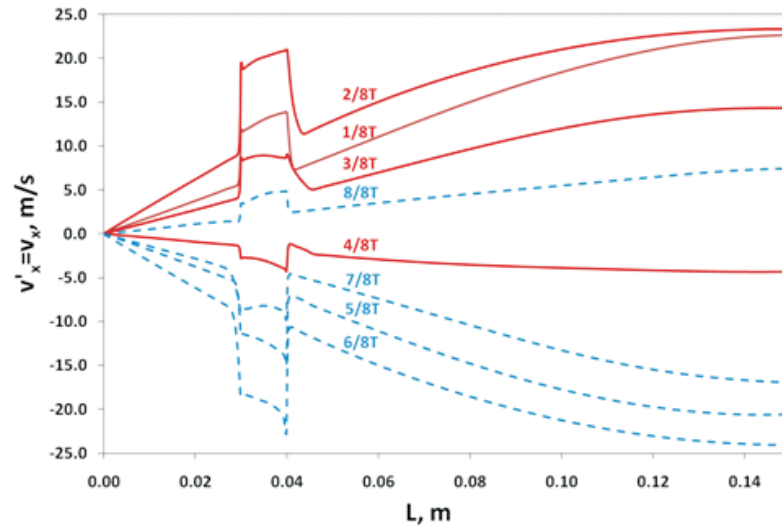


Figure 11. Distribution of instantaneous velocity depending on the length of the thermoacoustic engine.

Table 2. Comparison between simplified and detailed model of the thermoacoustic engine.

| x [m] | Amplitude | Simplified model | Detailed model | Difference | Relative error [%] |
|---------|-----------|------------------|----------------|------------|--------------------|
| 0.15 | v [m/s] | 24.46 | 20.96 | 3.5 | 16.7 |
| 0.0 | p [Pa] | 9491 | 8068 | 1423 | 17.6 |

of the thermoacoustic device in case of relative comparison of the specified variables.

Modelling of the few heating elements of heat exchanger allows also to capture the flow structure around the heating elements. Figure 12 presents the averaged distribution of velocity vectors around the heating elements of the heat exchanger.

The presence of heating elements causes large flow instabilities. The large vortices appear behind the heating elements. Additionally, the velocity in the axis of the heat exchanger channels is about 20–30% higher than near the walls of heating elements.

Figure 13 shows the v_x velocity distribution in function of time step for selected locations around the heat exchanger. The velocity amplitude

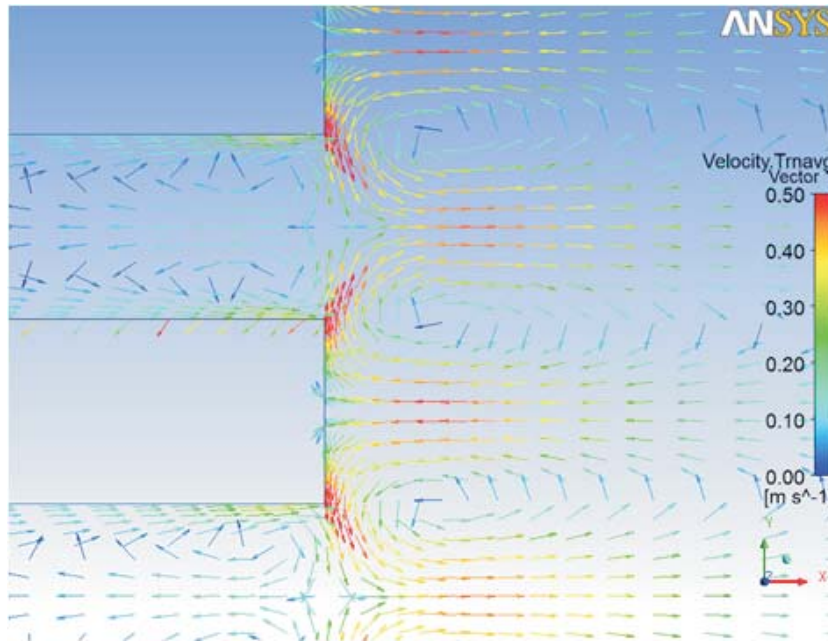


Figure 12. Distribution of the averaged velocity vectors around the heating elements for the detailed model of thermoacoustic device.

for monitor points located inside of the heat exchanger channel is equal to 15 m/s. The largest velocity amplitude is connected with point W4 which is located in the outlet cross-section of the heat exchanger and additionally this position is closer to the open end of the device which is simultaneously the antinode of velocity. The amplitude of the velocity for the monitor points outside of the heat exchanger is equal to 6 m/s for point W1 and 10 m/s for point W5. The distribution of the velocity in function of time step is not perfectly sinusoidal. The reason of this fact are non-linear effects which appear due to the presence of heat exchanger which may be the source of turbulence. Additionally, the velocity fluctuations are strongly coupled with the heat flux oscillations.

Figure 14 presents the FFT analysis of the v_x velocity component for two selected locations around the heat exchanger. The performed FFT analysis shows that beside of the main frequency component which is equal to about 600 Hz two additional components, equal to 1300 Hz and 1900 Hz, are visible. The first harmonic is higher for point W3 and reaches about 14 m/s. However, the second harmonic for point W3 is lower than in case

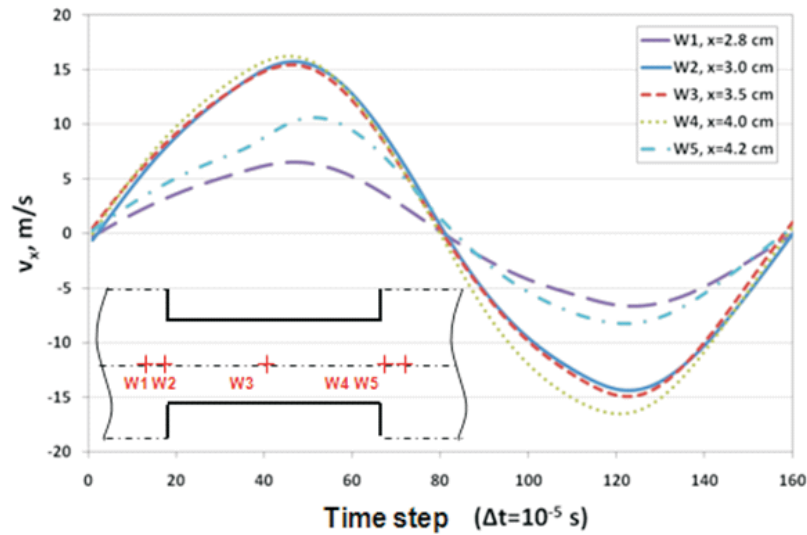


Figure 13. Distribution of the v_x velocity component along the single channel of heat exchanger.

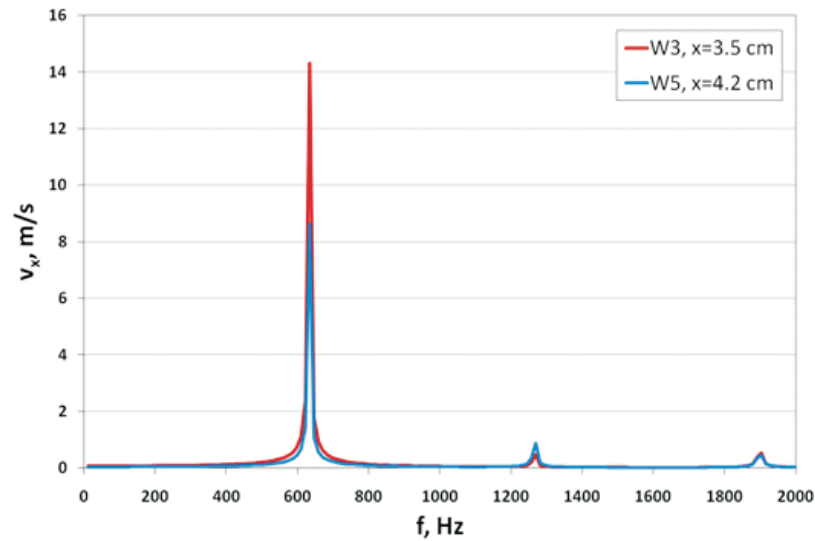


Figure 14. FFT analysis of the v_x velocity component for selected monitor points located around the heat exchanger.

of monitor point W5. This fact is connected with the position of point W5 near the large vortices outside the heat exchanger. The additional frequency components are responsible for the so called limit cycle for velocity, pressure and heat flux fluctuations.

3 Conclusions

Modelling the non-stationary flow field is a complicated process. It is also very time-consuming compared to the analysis of stationary problems. An additional difficulty in the presented calculations is the fact that the parameter change amplitude and the velocities of the flows are very small. This necessitates the use of sophisticated numerical methods and a search for solutions independent of the discretisation of the computational area.

The paper offers a detailed presentation of a methodology for the performance of calculations of the flow in the thermoacoustic engine, the way to discretise the computational area, the adoption of the initial boundary conditions and for the interpretation of results. The Authors believe that this type of modelling has a great potential for the future from the point of view of the effectiveness of the used numerical methods which are available in the commercial package CFD Ansys-CFX 12.

The presented results of the thermoacoustic engine calculations are the basis for further research on the improvements that can be made to this type of construction, and especially for studies aiming to optimise heat exchange – the shape of the exchanger, the temperature and the temperature gradient.

Acknowledgements The study presented in this paper was conducted within the framework of Research Project NN512316938 of the Polish Ministry of Science and Higher Education.

Received 10 October 2011

References

- [1] LORD RAYLEIGH: *The Theory of Sound*, Vol. II. Dover. New York 1945.
- [2] ROTT N.: *Damped and thermally driven acoustic oscillations in wide and narrow tubes*. Z. Angew. Math. Phys. **20**(1969), 230–243.

- [3] WHEATLEY J.T.: HOFER G.W., SWIFT A., MIGLIORI A.: *Understanding some simple phenomena in thermoacoustics with application to acoustical heat engines*. American Journal of Physics **53**(1985), 2, 147–162.
- [4] SWIFT G.W.: *Thermoacoustic Engines*. Journal of the Acoustical Society of America **84**(1988), 4, 1148–1180.
- [5] HANTSCHK C.C.: VORTMEYER D.: *Numerical simulation of self-excited thermoacoustic instabilities in a Rijke tube*. Journal of Sound and Vibration **277**(1999), 3, 511–522.
- [6] ZOONTJENS L.: *Numerical Investigations of the Performance and Effectiveness of Thermoacoustic Couples*. PhD thesis, The University of Adelaide, Adelaide 2008.
- [7] ZINK F., VIPPERMAN J., SCHAEFER L.: *CFD simulation of thermoacoustic cooling*. International Communications in Heat and Mass Transfer **37**(2010), 226–229.
- [8] DYKAS S., WRÓBLEWSKI W., RULIK S., CHMIELNIAK T.: *Numerical method for modelling of acoustic waves propagation*. Archives of Acoustics **35**(2010), 1, 35–49.
- [9] REMIORZ L., DYKAS L., RULIK S.: *Numerical modelling of the thermoacoustic phenomenon as a contribution to the model of the thermoacoustic engine*. TASK Quarterly **14**(2010), 3.